Dynamic higher-order equations for finite rods

DYNAMIC HIGHER ORDER EQUATIONS FOR FINITE RODS

by Peter D. Folkow [‡] *and* Karl Mauritsson [§]

(*Department of Applied Mechanics, Chalmers University of Technology, SE-412 96 Göteborg, Sweden*)

[Received October 2009.]

Summary

This work considers longitudinal wave propagation in circular cylindrical rods adopting Boström's power series expansion method in the radial coordinate. Equations of motion together with consistent sets of general lateral and end boundary conditions are derived in a systematic fashion up to arbitrary order using a generalized Hamilton's principle. Analytical comparisons are made between the present theory to low order and several classic theories. Numerical examples for eigenfrequencies, displacement and stress distributions are given for various sorts of finite rod structures. The results are presented for series expansion theories of different order and various classical theories, from which one may conclude that the present method generally models the rod accurately.

1. Introduction

There exist many models which describe the longitudinal elastodynamic wave propagation in finite circular cylindrical rods. It has been treated at different levels; from a simple one-dimensional wave propagation problem to the complete three-dimensional theory of elastodynamics, see for example (**1**) for a brief review. The involved three-dimensional theory has been adopted in conjunction with various levels of approximations when studying dynamic rod problems for different standard end boundary conditions. Most such works consider eigenfrequency analyzes using fix frequency. There exists on one hand analytical solutions based on expansion in terms of Bessel functions (**2**, **3**, **4**, **5**, **6**, **7**) where part of the boundary conditions are satisfied approximately, and on the other hand numerical solutions such as the Ritz method (**8**, **9**, **10**, **11**) or the finite element method (**12**, **13**).

[‡] Corresponding author, e-mail: peter.folkow@chalmers.se, Phone: +46 31 772 1521 , Fax: +46 31 772 3827

[§] e-mail: karl.mauritsson@chalmers.se, Phone: +46 31 772 3478 , Fax: +46 31 772 3827

However, the bulk of analysis has been on various approximate models due to the complexity of the exact theory. In these simplified theories, both the dynamic equations and the boundary conditions are often derived using various kinds of simplifying kinematic assumptions. The most used approximate theory is the simple one-dimensional wave equation (**1**), where radial effects are neglected. If the rod radius is much smaller than the wavelengths this approximation is known to yield accurate results. The next level is to include radial inertia in the derivation process described by Love (**14**). This leads to a slightly more involved differential equation that has the undesired feature of being nonhyperbolic. A more advanced theory is due to Mindlin and Hermann (**15**) (henceforth denoted the Mindlin-Hermann theory) where both radial inertia and radial shear are considered, resulting in a hyperbolic equation. Mindlin and McNiven (**16**) schematically derived an expansion theory of arbitrary order using Jacobi polynomials, where the so called second-order approximation involving three displacement terms was presented in detail (henceforth denoted the Mindlin-McNiven theory). Other such finite terms rod theories have been suggested ever since, of which most are based on similar approaches as the ones discussed above (**17**, **18**, **19**, **20**).

A higher order power series expansion of both displacements and frequencies was derived by Achenbach and Fang (**21**) for an infinite rod using the three-dimensional equations of motion, resulting in the rod frequency spectrum and the corresponding mode shapes. A seemingly similar approach was adopted by Boström (**22**) using a power series expansion of the displacement fields only, which subsequently resulted in a hierarchy of rod equations expressed in the time domain. Besides the mentioned work by Mindlin and McNiven, Achenbach and Fang, and Boström, there exist many other series expansion techniques for elastic structures (rods, plates, shells) that may be truncated to arbitrary order e.g. (**23**, **24**, **25**, **26**, **27**, **28**, **29**, **30**, **31**, **32**). Only a few of these works adopt the important concept of developing recursion relations (**22**, **21**, **30**, **31**, **32**), from which it is possible to reduce the number of displacement fields in a consequent manner. These latter work derive the equations of motion through the lateral boundary conditions, and hereby have the appealing property of exactly fulfilling these conditions. However, note that there are generally several additional differences in the derivation procedure among the works using recursion relations, such as the series expansion method, the procedure when collecting terms or the truncation process as a whole. One interesting exception here concerns isotropic plates, where the seemingly alternative method used

by Losin (**31**) actually results in the same equations of motion as when adopting the Boström method (**33**, **34**). Besides rods and plates, the Boström procedure has also been generalized to other structures such as shells (**35**), anisotropic rods (**36**, **37**), piezoelectric layers (**38**, **39**) and porous plates (**40**) (the latter work is influenced by Losin's method). In all these works, only the differential equations describing the wave propagation are derived without determining the pertinent end boundary conditions. Hence, there are needs to establish the corresponding boundary conditions in an equally systematic manner.

Traditionally, variational formulation methods are used when developing the end boundary equations. Of the works on arbitrary order theories for rods, plates and shells cited above, such boundary conditions have been presented in Refs. (**16**, **24**, **27**, **29**). These cited works mainly derive boundary conditions schematically for standard end conditions, where numerical results on finite structures are only presented by Matsunaga (**27**). Among these works, only Medick (**24**) derives both the traction and displacement boundary conditions in a equally systematic fashion using a generalized Hamilton's principle where displacements, stresses and strains are varied independently.

The present paper aims at developing the end boundary conditions in a systematic fashion up to an (in principle) arbitrary order for a rod according to the Boström theory. To this end a generalized Hamilton's principle is used, where both the displacements and the stresses are varied independently. This results in traction and displacement boundary conditions, as well as the rod equation of motion. The latter equation thus verifies that Boström's rod equation is variationally consistent. Moreover, it becomes more evident from the derivation procedure at which stages this method deviates from other series expansion theories adopting variational techniques. Concerning the pertinent end and lateral boundary conditions, these are presented in a quite general fashion that may be adopted on various sorts of rod structures. Besides presenting a hierarchy of rod equations with end boundary conditions, a more detailed comparison is performed between the lowest non-trivial Boström theory and the Mindlin-Hermann and Mindlin-McNiven theories. The numerical results present the three lowest eigenfrequencies for two sets of end boundary conditions, together with corresponding displacement and stress distributions. Two more involved boundary conditions are also briefly discussed.

2. Hamilton's principle

Consider a cylindrical rod with length L and radius a. The rod is homogeneous, isotropic and linearly elastic with density ρ and Lamé constants λ and μ. Cylindrical coordinates are used with axial coordinate x, radial coordinate r and circumferential coordinate θ. The displacement field is rotationally symmetric with axial component u_x and radial component u_r. A generalized Hamilton's principle can be used to derive the differential equation describing the motion of the rod and the corresponding boundary conditions. Here, the variation is extended from the ordinary Hamilton's principle by assuming simultaneous and independent variations of displacements and stresses. The concept is related to combinations of the principles of minimum energy and complementary energy, and has been used in several different versions for both elastostatics (**41**, **42**) and elastodynamics (**24**, **43**, **44**). The preferred method of presentation differs in some respects to the ones cited above, but results in the same final equations as if adopting Refs. (**24**, **43**, **44**) directly. The Hamilton's principle (**1**) states that

$$\delta \int_{t_0}^{t_1} L dt = 0, \qquad L = T - U + W, \tag{1}$$

where T is the kinetic energy, U is the potential energy and W is the work done by body forces and surface tractions. The energy densities $\overline{T}$ and $\overline{U}$ are defined as

$$\overline{T} = \rho/2\, \dot{\boldsymbol{u}} \cdot \dot{\boldsymbol{u}} = \rho/2 \left(\dot{u}_x^2 + \dot{u}_r^2\right), \qquad \overline{U} = 1/2\, \boldsymbol{\sigma} : \boldsymbol{\epsilon} = 1/2 \left(\sigma_{xx}\epsilon_{xx} + \sigma_{rr}\epsilon_{rr} + \sigma_{\theta\theta}\epsilon_{\theta\theta}\right) + \sigma_{xr}\epsilon_{xr}, \tag{2}$$

where $\boldsymbol{\sigma}$ is the stress, $\boldsymbol{\epsilon}$ is the strain and a dot denotes a time derivative. Note that $\{u_\theta, \epsilon_{x\theta}, \epsilon_{r\theta}, \sigma_{x\theta}, \sigma_{r\theta}\}$ are all zero due to the rotationally symmetric displacement field. Naturally, the strains are expressed in terms of the displacements according to $\boldsymbol{\epsilon} = 1/2(\nabla \boldsymbol{u} + \boldsymbol{u}\nabla)$. By considering displacement terms and force terms as independent, the variational expressions become

$$\delta \int_{t_0}^{t_1} T dt = -1/2 \int_{t_0}^{t_1} \int_V \rho \left(\ddot{\boldsymbol{u}} \cdot \delta \boldsymbol{u} + \boldsymbol{u} \cdot \delta \ddot{\boldsymbol{u}}\right) dV dt, \tag{3}$$

$$\delta \int_{t_0}^{t_1} U dt = 1/2 \int_{t_0}^{t_1} \int_V \left(\boldsymbol{\sigma} : \delta \boldsymbol{\epsilon} + \boldsymbol{\epsilon} : \delta \boldsymbol{\sigma}\right) dV dt, \tag{4}$$

$$\delta \int_{t_0}^{t_1} W dt = 1/2 \int_{t_0}^{t_1} \left(\int_V \rho \left(\boldsymbol{f} \cdot \delta \boldsymbol{u} + \boldsymbol{u} \cdot \delta \boldsymbol{f}\right)\, dV + \int_S \left(\boldsymbol{t} \cdot \delta \boldsymbol{u} + \boldsymbol{u} \cdot \delta \boldsymbol{t}\right)\, dS \right) dt, \tag{5}$$

where V is the volume and S is the surface of the rod, respectively. Adopting the divergence theorem on (4), together with prescribed displacement $\tilde{\boldsymbol{u}}$ on $S_{\boldsymbol{u}}$ and prescribed traction $\tilde{\boldsymbol{t}}$ on $S_{\boldsymbol{t}}$, the generalized

Hamilton's principle (1) may be reduced to the following rod equation on variational form:

$$\int_{t_0}^{t_1}\left(\int_V(\nabla\cdot\boldsymbol{\sigma}+\rho\boldsymbol{f}-\rho\ddot{\boldsymbol{u}})\cdot\delta\boldsymbol{u}\,dV+\int_{S_{\boldsymbol{t}}}\left(\tilde{\boldsymbol{t}}-\boldsymbol{n}\cdot\boldsymbol{\sigma}\right)\cdot\delta\boldsymbol{u}\,dS+\int_{S_{\boldsymbol{u}}}(\tilde{\boldsymbol{u}}-\boldsymbol{u})\cdot\delta\boldsymbol{t}\,dS\right)dt=0. \quad (6)$$

Since the virtual displacements δu_x and δu_r are independent in the interior and at the boundaries, and the virtual tractions δt_x and δt_r are independent at the boundaries, equation (6) reduces to separate equations for each variational term. In the present case of rotationally symmetric fields, it is natural to assume that $S_{\boldsymbol{u}}$ and $S_{\boldsymbol{t}}$ are composed of subregions such as cylindrical parts on the lateral surface $r=a$ and circular rings at the bases $x=0$ and $x=L$. Let a prescribed traction $\tilde{t}_x$ be given at $x\in L_x$ for $r=a$, at $r\in R_{0x}$ for $x=0$, and at $r\in R_{Lx}$ for $x=L$. Hence, the displacement $\tilde{u}_x$ is prescribed at the complementary parts denoted by $\{L_x^*,R_{0x}^*,R_{Lx}^*\}$. Similarly, $\tilde{t}_r$ is known at $\{L_r,R_{0r},R_{Lr}\}$ while $\tilde{u}_r$ is known at the complementary part $\{L_r^*,R_{0r}^*,R_{Lr}^*\}$. The equation (6) thus reduces to separate integrals

$$\int_0^L\int_0^a\left(\frac{\partial\sigma_{xx}}{\partial x}+\frac{\partial\sigma_{xr}}{\partial r}+\frac{\sigma_{xr}}{r}+\rho f_x-\rho\frac{\partial^2u_x}{\partial t^2}\right)\delta u_x r dr dx=0, \quad (7)$$

$$\int_0^L\int_0^a\left(\frac{\partial\sigma_{rr}}{\partial r}+\frac{\partial\sigma_{xr}}{\partial x}+\frac{\sigma_{rr}-\sigma_{\theta\theta}}{r}+\rho f_r-\rho\frac{\partial^2u_r}{\partial t^2}\right)\delta u_r r dr dx=0, \quad (8)$$

$$\int_{L_x}\left(\tilde{t}_x-\sigma_{xr}\right)\delta u_x dx=\int_{L_x^*}\left(\tilde{u}_x-u_x\right)\delta t_x dx=0, \qquad r=a, \quad (9)$$

$$\int_{L_r}\left(\tilde{t}_r-\sigma_{rr}\right)\delta u_r dx=\int_{L_r^*}\left(\tilde{u}_r-u_r\right)\delta t_r dx=0, \qquad r=a, \quad (10)$$

$$\int_{R_{\{0,L\}x}}\left(\tilde{t}_x\pm\sigma_{xx}\right)\delta u_x r dr=\int_{R^*_{\{0,L\}x}}\left(\tilde{u}_x-u_x\right)\delta t_x r dr=0, \qquad x=\{0,L\}, \quad (11)$$

$$\int_{R_{\{0,L\}r}}\left(\tilde{t}_r\pm\sigma_{xr}\right)\delta u_r r dr=0\int_{R^*_{\{0,L\}r}}\left(\tilde{u}_r-u_r\right)\delta t_r r dr=0, \qquad x=\{0,L\}. \quad (12)$$

The stresses in these equations may be expressed in terms of the displacements through

$$\begin{aligned}\sigma_{xx}&=\lambda\left[\frac{1}{r}\frac{\partial}{\partial r}(ru_r)+\frac{\partial u_x}{\partial x}\right]+2\mu\frac{\partial u_x}{\partial x}, &\qquad \sigma_{rr}&=\lambda\left[\frac{1}{r}\frac{\partial}{\partial r}(ru_r)+\frac{\partial u_x}{\partial x}\right]+2\mu\frac{\partial u_r}{\partial r},\\ \sigma_{\theta\theta}&=\lambda\left[\frac{1}{r}\frac{\partial}{\partial r}(ru_r)+\frac{\partial u_x}{\partial x}\right]+2\mu\frac{u_r}{r}, &\qquad \sigma_{xr}&=\mu\left[\frac{\partial u_x}{\partial r}+\frac{\partial u_r}{\partial x}\right].\end{aligned} \quad (13)$$

3. Equations of motion

In conformity with **(22)** the fields are expanded in power series according to

$$u_x=u_0(x,t)+r^2u_2(x,t)+r^4u_4(x,t)+\ldots, \qquad u_r=ru_1(x,t)+r^3u_3(x,t)+r^5u_5(x,t)+\ldots, \quad (14)$$

where the even and odd expansions are due to a correct behavior at $r = 0$. Here it is assumed that u_i are smooth with continuous derivatives (**30**). Substituting these expansions in the stress expressions (13) gives

$$\sigma_{jj} = \sigma_{jj,0}(x,t) + r^2\sigma_{jj,2}(x,t) + \ldots, \qquad \sigma_{xr} = r\sigma_{xr,1}(x,t) + r^3\sigma_{xr,3}(x,t) + \ldots, \tag{15}$$

where j is $\{x, r, \theta\}$, respectively. The terms are explicitly written

$$\begin{aligned} &\sigma_{xx,2k} = (\lambda+2\mu)u'_{2k} + 2(k+1)\lambda u_{2k+1}, \qquad &&\sigma_{rr,2k} = \lambda u'_{2k} + (2(k+1)(\lambda+\mu) + 2k\mu)\, u_{2k+1}, \\ &\sigma_{\theta\theta,2k} = \lambda u'_{2k} + (2(k+1)\lambda + 2\mu)\, u_{2k+1}, \qquad &&\sigma_{xr,2k+1} = \mu u'_{2k+1} + 2(k+1)\mu u_{2k+2}, \end{aligned} \tag{16}$$

for $k = 0, 1, 2 \ldots$. Here a prime denotes an x-derivative.

3.1 *Recursion formulas*

Now, the power series expansions may be used in (7) and (8). Consider from now on no volume forces; $f_x = f_r = 0$. The expression inside the parentheses in (7) is an even function in r and denoted by $F_x = F_0 + r^2F_2 + \ldots$, while the corresponding parentheses in (8) is an odd function in r and denoted by $F_r = rF_1 + r^3F_3 + \ldots$. Hence, (7) and (8) hold provided that

$$\int_0^a \left(F_0 + r^2F_2 + \ldots\right)\left(\delta u_0 + r^2\delta u_2 + \ldots\right) r dr = 0, \tag{17}$$

$$\int_0^a \left(rF_1 + r^3F_3 + \ldots\right)\left(r\delta u_1 + r^3\delta u_3 + \ldots\right) r dr = 0. \tag{18}$$

For an expansion of equation (17) involving terms up to and including order $2m$, this involves $m+1$ unknowns $\{F_0, \ldots, F_{2m}\}$ and $m+1$ equations due to independent virtual displacement $\{\delta u_0, \ldots, \delta u_{2m}\}$. A corresponding situation holds for equation (18). Hence, the unique solutions of these equation systems are that each term in the series must vanish, i.e. $F_k = 0$ for $k = 1, 2, 3, \ldots$. Written in terms of the displacements, each such term is expressed as

$$\begin{aligned} u_{k+2} &= \frac{1}{(k+2)^2\mu}\left[\rho\ddot{u}_k - (\lambda+2\mu)u''_k - (k+2)(\lambda+\mu)u'_{k+1}\right], &&k = 0, 2, \ldots, \\ u_{k+2} &= \frac{1}{(k+1)(k+3)(\lambda+2\mu)}\left[\rho\ddot{u}_k - \mu u''_k - (k+1)(\lambda+\mu)u'_{k+1}\right], &&k = 1, 3, \ldots. \end{aligned} \tag{19}$$

These equations are recursion formulas also given by Boström (**22**). By using equation (19) all expressions involving $u_2, u_3, \ldots$ and derivatives thereof may thus be written in terms of u_0, u_1 and their derivatives. Note that the recursion formulas are exact provided that the displacement fields may be expanded in infinite

power series (14). Moreover, no truncations of the displacement terms have so far been performed, which is of crucial importance for the present method.

3.2 *Lateral boundary conditions*

The lateral boundary conditions are obtained directly from equations (9) and (10). Adopting the power series expansions (15), the tangential direction results in

$$a\,\sigma_{xr,1}(x,t) + a^3\sigma_{xr,3}(x,t) + \ldots = \tilde{t}_x(x,t), \qquad x \in L_x, \tag{20}$$

$$u_0(x,t) + a^2 u_2(x,t) + \ldots = \tilde{u}_x(x,t), \qquad x \in L_x^*, \tag{21}$$

and the normal direction in

$$\sigma_{rr,0}(x,t) + a^2\sigma_{rr,2}(x,t) + \ldots = \tilde{t}_r(x,t), \qquad x \in L_r, \tag{22}$$

$$a\,u_1(x,t) + a^3 u_3(x,t) + \ldots = \tilde{u}_r(x,t), \qquad x \in L_r^*. \tag{23}$$

These lateral boundary conditions actually constitute the hyperbolic rod equations of motion. Hence, different parts along the rod will in the general case be solved using different sets of differential equations. By adopting the recursion formulas (19) it is clear that (20)–(21) involve even order time and space derivatives on u_0, while (22)–(23) involve even order time and space derivatives on u_1. To obtain consistent sets of rod equations, a differential order $2m+2$ on u_0 (that is u_{2m+2}-terms) in (20)–(21) is to be paired to a differential order $2m$ on u_1 (that is u_{2m+1}-terms) in (22)–(23). This implies using $m+1$ terms in (20), (22), (23) and $m+2$ terms in (21), see further in Section 6.3. Equations (20) and (22) for lower order expansions are also given by Boström (**22**). Note that no truncations of the displacement terms are performed within each expanded stress field. As an illustration, series expansion of σ_{xr} up to $\sigma_{xr,2m+1}$ involves displacement terms up to u_{2m+2} according to (16). It is hereby important to initially keep a sufficient numbers of displacement terms before performing the subsequent truncations. It could be noted that the lateral boundary conditions are per definition fulfilled exactly for the expansion order in question, see more below.

4. End boundary conditions

The end boundary conditions are obtained from (11) and (12). Initially, it will be assumed that either $\tilde{t}_x$ or $\tilde{u}_x$, together with either $\tilde{t}_r$ or $\tilde{u}_r$, are given throughout each end boundary. The more general case where these end conditions are different for various subregions (rings) will be discussed briefly in Section 6.3. As both ends are to be treated in an analogous way, only the right end $x = L$ is discussed below. Moreover, consider the case when $\tilde{t}_x$ and $\tilde{t}_r$ are known, as given displacement end conditions are treated in the same general fashion. The integrals in (11) and (12) with $R_{Lx} = R_{Lr} = [0, a]$ hereby become

$$\int_0^a \left(\tilde{t}_x - (\sigma_{xx,0} + r^2\sigma_{xx,2} + \ldots)\right)\left(\delta u_0 + r^2\delta u_2 + \ldots\right) rdr = 0, \tag{24}$$

$$\int_0^a \left(\tilde{t}_r - (r\sigma_{xr,1} + r^3\sigma_{xr,3} + \ldots)\right)\left(r\delta u_1 + r^3\delta u_3 + \ldots\right) rdr = 0, \tag{25}$$

using the series representations in (16). Considering (24) it is thus straightforward to derive the $m + 1$ unknowns $\{\sigma_{xx,0}, \ldots, \sigma_{xx,2m}\}$ from the system of $m + 1$ equations for independent virtual displacement $\{\delta u_0, \ldots, \delta u_{2m}\}$. It is interesting to note that the hereby obtained representation of the boundary stress function σ_{xx} in power series is actually identical to the expansion of the given function $\tilde{t}_x$ in terms of shifted Legendre polynomials $P_k\left(1 - 2(r/a)^2\right)$ of order m. This may alternatively be expressed using Jacobi polynomials since $P_k^{(0,0)}(z) = P_k(z)$. In a similar fashion, (25) solved as a system of $m + 1$ unknowns renders that the series expanded boundary stress function σ_{xr}/r is identical to expanding $\tilde{t}_r/r$ in Jacobi polynomials $P_k^{(1,0)}\left(1 - 2(r/a)^2\right)$ of order m. Note that the functions σ_{xx} and σ_{xr} may also be obtained in a direct fashion through expanding $\tilde{t}_x$ and $\tilde{t}_r$ in Zernike polynomials $R_{2k}^0(r/a)$ and $R_{2k+1}^1(r/a)$, respectively. Clearly, this causes among others that the often studied case where the prescribed end boundary stresses (or displacements) are zero over the whole surface renders that each term in the corresponding series expansion is hereby zero. It could be noted that the Mindlin-McNiven theory (**16**) is based on expressing the series expansion fields corresponding to (14) in Jacobi polynomials.

In line with the differential order system discussed above for the lateral boundary conditions, the end boundary stresses should at most involve x-derivatives of orders $2m + 1$ on u_0 for σ_{xx} and $2m - 1$ on u_1 for σ_{xr} (a negative order implies no contribution). This is equivalent to say one order less than in the corresponding equation of motion. Hence, $m + 1$ terms should be used in the normal direction (24) and

m terms in the tangential direction (25). In the case of displacement end conditions, the same division holds between the number of terms in the normal and tangential directions, respectively. Hereby, the end boundary displacements involve x-derivatives of orders $2m$ on u_0 for u_x and $2m-2$ on u_1 for u_r at the most. This is as expected since being two order less than in the corresponding equation of motion. The all in all number of $4m+2$ end boundary conditions are in line with the (20)–(23), involving differential orders $2m+2$ on u_0 and $2m$ on u_1. Put in other words, by eliminating one of the fields, say u_1, this results in one differential equation for u_0 expressed in terms of partial derivatives in space and time of order $4m+2$.

4.1 *Coupling conditions*

When homogeneous rods with different properties (material, radius, lateral boundary condition) are merged together, there are $4m+2$ coupling conditions to be fulfilled: $m+1$ conditions on both u_x and σ_{xx}, as well as m conditions on both u_r and σ_{xr}. Of course, exact theory requires pointwise continuity on displacements and stresses. For the expansion theory, the continuity conditions on normal stresses and displacement are obtained from generalizations of (11)

$$\int_0^{a^l} \left(\sigma^l_{xx,0} + r^2\sigma^l_{xx,2} + \ldots\right)\left(\delta u_0 + r^2\delta u_2 + \ldots\right) r dr = \int_0^{a^r} \left(\sigma^r_{xx,0} + \ldots\right)\left(\delta u_0 + \ldots\right) r dr, \quad (26)$$

$$\int_0^{a^{lr}} \left(u^l_0 + r^2 u^l_2 + \ldots\right)\left(\delta\sigma_{xx,0} + r^2\delta\sigma_{xx,2} + \ldots\right) r dr = \int_0^{a^{lr}} \left(u^r_0 + \ldots\right)\left(\delta\sigma_{xx,0} + \ldots\right) r dr. \quad (27)$$

Here the superscript "l" is for the left-hand fields and "r" is for the right-hand fields, while the notation a^{lr} is $min\{a^l, a^r\}$. The same procedure holds for the tangential direction (12). Clearly, the displacement conditions result in termwise equality $u^l_k = u^r_k$ for $k = 0, 1, \cdots, 2m$ while the stress conditions are generalized force continuity requirements. In the special case $a^l = a^r$ each stress component is equal on both sides.

When calculating displacements and stresses anywhere in the rod, the number of terms used in (14)–(15) could be chosen in two different ways. One possibility is to consequently adopt $m+1$ terms for even order expanded fields $\{u_x, \sigma_{xx}, \sigma_{rr}, \sigma_{\theta\theta}\}$ and m terms for odd order expanded fields $\{u_r, \sigma_{xr}\}$. Hereby the end (and coupling) conditions are fulfilled in accordance to the presentation above, but the higher order lateral boundary conditions are not treated properly. Another possibility is to use the same number of fields as in the lateral boundary conditions, that is $m+1$ terms for all fields except u_x where $m+2$ terms are to be

used. Consequently, terms up to u_{2m+2} are hereby taken into account in all fields. Naturally, this causes the lateral boundary conditions to be fulfilled exactly, but corrupts the end (and coupling) conditions except for σ_{xx}. From the numerical examples in Section 6, it is shown that the latter approach is clearly superior to the former approach in the inner regions (including of course the lateral boundary). Close to or even at the end (and coupling) boundaries, the discrepancies due to an extra term in certain fields are either negligible or small in most cases. Hence, the latter approach is recommended and adopted throughout the paper.

5. Analytical comparisons

This section compares the equations of motion and standard end boundary conditions using the present theory and different classical theories such as the rod wave equation, the Love theory, the Mindlin-Hermann theory, and the Mindlin-McNiven theory. For simplicity, assume the standard situation with free lateral surface.

5.1 *Equations of motion*

In the exact case, the three dimensional solutions can, for fixed frequency ω, be given as (**45**)

$$\begin{aligned} u_x &= [Ak_x J_0(q_p r)\cos k_x x + Bq_s J_0(q_s r)\sin k_x x]e^{-i\omega t}, \\ u_r &= [Cq_p J_1(q_p r)\cos k_x x + Dk_x J_1(q_s r)\sin k_x x]e^{-i\omega t}, \end{aligned} \tag{28}$$

where J_0 and J_1 are Bessel functions, while k_x is the wavenumber in the x-direction and

$$\begin{aligned} q_p &= \sqrt{k_p^2 - k_x^2}, \qquad & k_p &= \omega\sqrt{\rho/(\lambda+2\mu)}, \\ q_s &= \sqrt{k_s^2 - k_x^2}, \qquad & k_s &= \omega\sqrt{\rho/(\mu)}. \end{aligned} \tag{29}$$

Two things could be stressed in association with these exact equations. Firstly, by performing a radial Maclaurin series expansion of the Bessel functions in (28), resulting in series like (14), these fields are shown to fulfill the recursion formulas (19). Secondly, and more important, by studying the dispersion relations analytically for exact and Boström's theory (**22**) more in detail, it is seen that a series expansion of the Pochhammer-Chree frequency equation renders the same terms as for the present theory, at least for the few lowest terms studied (see comparable situation for plates (**46**)). Hence, this is an indication that Boström's systematical approach probably is asymptotically correct.

The present theory is obtained from the equations of motion (20) and (22) for $L_x = L_r = (0, L)$

and $\tilde{t}_x = \tilde{t}_r = 0$ at $r = a$. Consider the case where two terms are included in each equation ($m = 1$), henceforth denoted the a^2-equation. These equations, although given in (**22**), are presented below to simplify comparisons. Thus

$$(\lambda+2\mu)\frac{\partial^2 u_0}{\partial x^2} - \rho\frac{\partial^2 u_0}{\partial t^2} + 2\lambda\frac{\partial u_1}{\partial x} + \frac{a^2}{4}\left[-\frac{3\lambda+4\mu}{2}\frac{\partial^4 u_0}{\partial x^4} - \frac{\rho^2}{2\mu}\frac{\partial^4 u_0}{\partial t^4} + \frac{\rho(\lambda^2+7\lambda\mu+8\mu^2)}{2\mu(\lambda+2\mu)}\frac{\partial^4 u_0}{\partial x^2\partial t^2} - (3\lambda+2\mu)\frac{\partial^3 u_1}{\partial x^3} + \frac{\rho(\lambda^2+4\lambda\mu+2\mu^2)}{\mu(\lambda+2\mu)}\frac{\partial^3 u_1}{\partial x\partial t^2}\right] = 0, \tag{30}$$

$$\lambda\frac{\partial u_0}{\partial x} + 2(\lambda+\mu)u_1 + \frac{a^2}{4}\left[\frac{\lambda+3\mu}{2}\frac{\partial^3 u_0}{\partial x^3} - \frac{\rho(\lambda+3\mu)}{2(\lambda+2\mu)}\frac{\partial^3 u_0}{\partial x\partial t^2} + \lambda\frac{\partial^2 u_1}{\partial x^2} + \frac{\rho(2\lambda+3\mu)}{\lambda+2\mu}\frac{\partial^2 u_1}{\partial t^2}\right] = 0. \tag{31}$$

Consider next the classical rod theory

$$c_E^2\frac{\partial^2 u_0}{\partial x^2} - \frac{\partial^2 u_0}{\partial t^2} = 0, \tag{32}$$

where $c_E = \sqrt{E/\rho}$ and E is Young's modulus. Taking radial inertia into account results in the Love theory (**1**)

$$c_E^2\frac{\partial^2 u_0}{\partial x^2} - \frac{\partial^2 u_0}{\partial t^2} + \frac{\nu^2 a^2}{2}\frac{\partial^4 u_0}{\partial x^2\partial t^2} = 0, \tag{33}$$

where ν is Poisson's ratio. Equation (32) is identical to the parts of order a^0 in equations (30) and (31) when the field u_1 is eliminated (**22**). Hence, this is henceforth referred to as the a^0-equation. The Love equation involves an extra term of order a^2, which corresponds to a similar term when eliminating u_1 in (30) and (31), see further below. The Mindlin-Hermann theory (**15**) considers both radial inertia and radial shear

$$(\lambda+2\mu)\frac{\partial^2 u_0}{\partial x^2} - \rho\frac{\partial^2 u_0}{\partial t^2} + 2\lambda\frac{\partial u_1}{\partial x} = 0, \tag{34}$$

$$\lambda\kappa_0^2\frac{\partial u_0}{\partial x} + 2(\lambda+\mu)\kappa_0^2 u_1 + \frac{a^2}{4}\left(-\mu\kappa^2\frac{\partial^2 u_1}{\partial x^2} + \rho\frac{\partial^2 u_1}{\partial t^2}\right) = 0. \tag{35}$$

Here κ and κ_0 are adjustments constants. In the numerical results, these constants are chosen as $\kappa = 0.93$ and $\kappa_0 = 0.69$ as suggested in (**15**). It is interesting to compare this latter set of equations analytically to the series expansion equations. Considering (34) this is identical to the a^0-expansion in (30). Equation (35) (divided by κ_0^2) has the same a^0-terms as (31), while the a^2-terms only involve u_1-terms which differ in magnitude and even sign in the first term. Clearly, no a^2-terms are present in (34). Hence, there are several differences between these two theories for an expansion of order a^2.

Finally, the three mode theory according to Mindlin-McNiven (**16**) also considers axial shear deformation. These equations, originally expressed using Jacobi polynomials, are here formulated in terms of the power series expansion (14) as

$$(\lambda+2\mu)\frac{\partial^2 u_0}{\partial x^2}-\rho\frac{\partial^2 u_0}{\partial t^2}+2\lambda\kappa_1\frac{\partial u_1}{\partial x}+\frac{a^2}{2}\left((\lambda+2\mu)\frac{\partial^2 u_2}{\partial x^2}-\rho\frac{\partial^2 u_2}{\partial t^2}\right)=0, \tag{36}$$

$$\lambda\kappa_1\frac{\partial u_0}{\partial x}+2(\lambda+\mu)\kappa_1^2 u_1+\frac{a^2}{4}\left(-\mu\kappa_2^2\frac{\partial^2 u_1}{\partial x^2}+\rho\kappa_3^2\frac{\partial^2 u_1}{\partial t^2}-2(\mu\kappa_2^2-\lambda\kappa_1)\frac{\partial u_2}{\partial x}\right)=0, \tag{37}$$

$$\mu\kappa_2^2\frac{\partial u_1}{\partial x}+2\mu\kappa_2^2 u_2+\frac{a^2}{12}\left(-(\lambda+2\mu)\frac{\partial^2 u_2}{\partial x^2}+\rho\kappa_4^2\frac{\partial^2 u_2}{\partial t^2}\right)=0, \tag{38}$$

where κ_i are adjustments constants generally chosen so as to minimize the long wavelength error for the three branches of the dispersion curves. In the numerics, these are chosen as $\kappa_1 = 0.89$, $\kappa_2 = 1.18$, $\kappa_3 = 1.00$ and $\kappa_4 = 1.51$ for $\nu = 0.3$ according to (**16**). There are several similarities between the first two equations (36)–(37), the Mindlin-Hermann equations (34)–(35) and the present theory (30)–(31). These similarities could have been seen more readily by writing the Mindlin-McNiven equations as a system of two equations through elimination of the u_2 field. However, as there are numerous different ways to express such a set of equations (even for a common set of a^0-terms) (**39**) this process is not pursued here. Instead, the set of equations are turned into one single equation in terms of the u_0 field. Such representations are also presented for the Mindlin-Hermann theory in (**15**) and for the series expansion a^2-theory in (**22**), respectively. All these cases result in the following general equation form

$$\frac{1}{c_E^2}\frac{\partial^2 u_0}{\partial t^2}-\frac{\partial^2 u_0}{\partial x^2}+a^2\left(\frac{b_1}{c_E^4}\frac{\partial^4 u_0}{\partial t^4}-\frac{b_2}{c_E^2}\frac{\partial^4 u_0}{\partial t^2\partial x^2}+b_3\frac{\partial^4 u_0}{\partial x^4}\right)+\mathcal{O}\big(a^4\big)=0. \tag{39}$$

Note that the Mindlin-Hermann case here involves no a^4-terms contrary to the series expansion and Mindlin-McNiven theories. It is seen that all theories are identical concerning terms of order a^0 (the classical wave equation), and involve the same differential orders for the three a^2-terms. However, the positive coefficients b_j differ somewhat in all the different theories. Using standard material parameters, e.g. steel, as well as the numerical values for κ and the various κ_i, all three coefficients b_j in the a^2-theory are roughly twice as big as in the Mindlin-McNiven theory. When compared to the Mindlin-Hermann theory, these coefficients are approximately four times greater in the a^2-theory. As a further comparison between different theories, the term b_2 in the series expansion theory is approximately 16 times greater than

the corresponding term in Love's theory (33). The effects from these discrepancies are further manifested in the numerical results.

5.2 *Standard end boundary conditions*

Here comparisons are made between the different theories for various standard end boundary conditions such as combinations of free and fixed ends. As for the analytical expressions for the equations of motion discussed above, only the a^2-theory is described for the series expansion theory. The total number of three boundary conditions on each end are thus divided into two conditions on u_x or σ_{xx}, as well as one condition on u_r or σ_{xr}. A rod fixed in the x-direction results in $u_0 = 0$ and $u_2 = 0$, while a fixation in the r-direction results in $u_1 = 0$. Consequently, a rod free to move in the x-direction results in $\sigma_{xx,0} = 0$ and $\sigma_{xx,2} = 0$ which by using (16) becomes

$$(\lambda + 2\mu)u_0' + 2\lambda u_1 = 0, \qquad (\lambda + 2\mu)u_2' + 4\lambda u_3 = 0, \tag{40}$$

while the corresponding situation in the r-direction results in $\sigma_{xr,1} = 0$ which corresponds to

$$u_1' + 2u_2 = 0. \tag{41}$$

When applying these boundary conditions for a solution to the rod equation of motion, the recursion formulas (19) are adopted on the terms involving u_2 and u_3, giving boundary conditions in terms of u_0 and u_1 only.

The single boundary conditions on each end for both the classical rod theory and the Love theory only considers the behavior in the x-direction. Hence, a rod fixed in the x-direction results in $u_0 = 0$ while a rod free to move in the x-direction results in $u_0' = 0$. These well known results are found among the series expansion relations above if only the u_0 displacement is considered. (However, note that both u_2 and u_3 actually involve u_0 implicitly through the recursion relations).

In the Mindlin-Hermann theory one needs two boundary conditions at each end comprising both longitudinal and radial effects. Fixed ends in the x- or r-direction correspond to $u_0 = 0$ and $u_1 = 0$, respectively. Free ends in the x-direction corresponds to $(\lambda + 2\mu)u_0' + 2\lambda u_1 = 0$ while free ends in the r-direction returns $u_1' = 0$. Again, these cases are found among (40) and (41), provided that terms u_2 and higher are omitted.

Finally, there must be three boundary conditions at each end for the Mindlin-McNiven theory, just as for the series expansion theory. As is expected, a rod fixed in the x-direction results in $u_0 = 0$ and $u_2 = 0$, while a fixation in the r-direction results in $u_1 = 0$. For unrestrained motion in the x-direction one has $(\lambda+2\mu)u_0' + 2\lambda\kappa_1 u_1 = 0$ and $u_2' = 0$ while the corresponding situation in r-direction gives $u_1' + 2u_2 = 0$. Similar results are given in (40) and (41) if u_3 is disregarded. Note that the Mindlin-McNiven theory involves the correction factor κ_1, which is often chosen slightly less than unity.

6. Numerical examples

In this section, the eigenfrequencies and the stress distribution for the series expansions theories are compared with one another using different truncation orders. These expansions are also compared to other classical theories as well as the exact theory. As in Section 5 mainly a free lateral surface and simple end boundary conditions are studied. Other more complicated cases are briefly discussed in Section 6.3. Two different end conditions are considered in Sections 6.1 and 6.2: mixed boundary conditions where the rod is fixed in axial direction and free in radial direction (guided ends), and clamped boundary conditions, respectively. Such end conditions have been studied by others using approximate techniques based on three-dimensional analysis. Liew and Hung (**9**) used the Ritz minimum energy principle, Buchanan (**13**) used the finite element method while Kari (**7**) adopted a wave guide model with mode matching. The present paper calculates the three lowest eigenfrequencies for two different length to radius ratios: $a/L = 1/20$ and $a/L = 1/4$. These cases are also studied in by Liew and Hung (**9**), which makes it natural to use the same normalization frequency $\Omega = \omega a/c_E$ as in (**9**). The comparisons are made in terms of the relative error. When the absolute value of the relative error is less than 10^{-4}, this is marked by a star $(*)$. Note that the three-dimensional mixed boundary case can be solved analytically rendering the exact results, contrary to the clamped boundary case. Therefore, comparisons to the exact results in the latter case are obtained using higher order approximate methods that are expected to have converged to an accurate level. The different series expansion theories are in Sections 6.1 and 6.2 denoted through the radius power a^{2m} in line with (30)–(31), involving time and space derivatives of orders $2m+2$ on u_0 and $2m$ on u_1, respectively.

When displaying the stress distribution in a rod, only the lowest eigenfrequency with $a/L = 1/4$ is

presented for the two boundary cases, respectively. The main reason for this is that this case readily illustrates the qualitative accuracies for the different theories; features that are appearing in a similar way in the higher modes and for other length to radius ratios. The plots will focus on the three stresses σ_{xx}, σ_{rr} and σ_{xr}. Especially, σ_{rr} and σ_{xr} are of interest to illustrate whether the lateral stress boundary conditions are adequately met for the classical theories. The eigenmodes are generally normalized so that the maximum longitudinal displacement u_x at $r = 0$ is equal to unity. For the boundary conditions considered in Sections 6.1 and 6.2, this occurs at $x = L/2$ for the first eigenmode.

6.1 *Mixed boundary conditions*

Consider first the mixed boundary condition $u_x = 0$ and $\sigma_{xr} = 0$ at $x = 0, L$. For a series expansion theory a^{2m} this implies at both ends that the $m + 1$ terms $u_{2k} = 0$ and the m terms $\sigma_{xr,2k-1} = 0$ for $k = 0, \cdots, m$ in accordance to Section 4. Table 1 presents the three lowest eigenfrequencies for $a/L = 1/20$ and $a/L = 1/4$, respectively. Here, the exact theory is compared to series expansion theories of order a^0, a^2, a^4 and a^6. These results show how the accuracy of the series solution is improved as the a^{2m} order is increased. It is also seen that the accuracies are inferior for higher eigenfrequencies as expected. Moreover, the results for slender rods, $a/L = 1/20$, are superior to the ones when $a/L = 1/4$. Of course, the results from the a^0-expansion are not affected by the ratio a/L for fixed L.

Table 2 gives the eigenfrequencies for exact theory and the relative error for the approximate theories: Love, Mindlin-Hermann (M-H), and Mindlin-McNiven (M-McN). Here the results for the a^2-theory are also included in order to clarify comparisons. These results show that the a^2 series expansions theory generally is superior to the traditional theories, especially for a slender rod $a/L = 1/20$. However, it is surprising that the quite simple Love theory mainly renders more accurate results than both the Mindlin-Hermann and the Mindlin-McNiven theories. The high accuracy of the Love theory here is probably due to the specific choice of boundary conditions with vanishing shear stresses, as such stresses are not taken into account in this theory. Note that the accuracies using both the Mindlin-Hermann and the Mindlin-McNiven theories depend on the choice of adjustments constants κ and κ_i, see Section 5.1.

Next, the distribution of stresses is displayed using the a^2 and classical theories for the lowest mode when $a/L = 1/4$. Figure 1(a) considers the variation of σ_{rr} along the rod for $r = 0$ for different theories.

a/L	Ω	Exact	a^0	a^2	a^4	a^6
$1/20$	Ω_1	0.3140	6×10^{-4}	$*$	$*$	$*$
	Ω_2	0.6269	2.2×10^{-3}	$*$	$*$	$*$
	Ω_3	0.9376	5.2×10^{-3}	-1×10^{-4}	$*$	$*$
$1/4$	Ω_1	1.5467	1.56×10^{-2}	-1.4×10^{-3}	$*$	$*$
	Ω_2	2.8857	8.87×10^{-2}	-3.17×10^{-2}	3.2×10^{-3}	-2×10^{-4}
	Ω_3	3.7142	2.688×10^{-1}	3.30×10^{-2}	1.04×10^{-2}	-5×10^{-4}

Table 1 Mixed boundary conditions: The eigenfrequencies for exact theory and the relative error for series expansion theories of order a^0, a^2, a^4 and a^6.

a/L	Ω	Exact	Love	M-H	M-McN	a^2
$1/20$	Ω_1	0.3140	$*$	-3×10^{-4}	-3×10^{-4}	$*$
	Ω_2	0.6269	$*$	-8×10^{-4}	-6×10^{-4}	$*$
	Ω_3	0.9376	2×10^{-4}	-1.9×10^{-3}	-1.4×10^{-3}	-1×10^{-4}
$1/4$	Ω_1	1.5467	1.7×10^{-3}	-5.2×10^{-3}	-4.1×10^{-3}	-1.4×10^{-3}
	Ω_2	2.8857	3.29×10^{-2}	-9.3×10^{-3}	-1.94×10^{-2}	-3.17×10^{-2}
	Ω_3	3.7142	1.349×10^{-1}	3.13×10^{-2}	-2.44×10^{-2}	3.30×10^{-2}

Table 2 Mixed boundary conditions: The eigenfrequencies for exact theory and the relative error for approximate theories: Love, Mindlin-Hermann (M-H), Mindlin-McNiven (M-McN) and a^2-theory.

The a^2-theory is more accurate than the Mindlin-McNiven theory, which in turn renders better results than the Mindlin-Hermann theory. Note that the a^0 and the Love theories do not model this stress component. The same accuracy sequence between theories are obtained for σ_{xx} (which both a^0 and Love theories model) but here the variation between all the theories are less pronounced and thus not displayed, see more below.

Figure 1(b) presents σ_{xr} along the rod for $r = a$, and thus illustrates how well the different theories fulfil the lateral shear boundary condition. It is seen that the shear stress using the Mindlin-McNiven theory is considerably better that both the Mindlin-Hermann and the Love theories (a^0 do not model this stress component). However, the Mindlin-McNiven stresses are not negligible, especially when compared to the a^2-theory that fulfils this boundary condition exactly. Note that all displayed theories seem to fulfil the end

boundary conditions for $r = a$, see more below. The general situation is quite similar for the normal stress σ_{rr} along the lateral boundary (not displayed here), where the a^2-theory renders the exact result. Here both the Mindlin-McNiven and the Mindlin-Hermann theories present stress levels that are comparable to the ones obtained for $r = 0$ in Fig. 1(a), which thus implies a deterioration for the Mindlin-McNiven theory when compared to the shear boundary condition in Fig. 1(b).

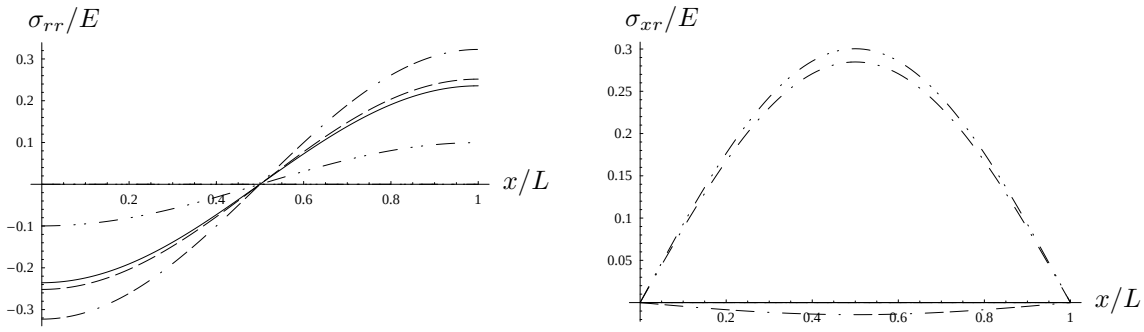

(a) σ_{rr} at $r = 0$.

(b) σ_{xr} at $r = a$.

Fig. 1 Mixed boundary conditions: —— Exact, $---$ a^2, $--\cdot--$ M-McN, $-\cdot\cdot-$ M-H, $-\cdot-$ Love.

The behavior at the end $x = L$ is given in Figures 2 for σ_{xx} and σ_{rr}, respectively. Both figures show the improved accuracy using the proposed series expansion theory of order a^2 compared to the classical theories. Note that the results from the a^0 and Love theories are on a common lowest horizontal line in Fig. 2(a). Figure 2(b) also displays the behavior at the lateral boundary $r = a$ in a clear manner. As the shear stress boundary conditions at the ends are fulfilled rather accurately for all theories, these results are not presented here.

No displacement plots are given here as there are no significant differences between the theories, albeit the a^2 theory is the most accurate. As mentioned before, higher modes and a more slender rod $a/L = 1/20$ generally show the same mutual accuracy relations between the theories as presented above. Surprisingly, for certain stress terms the Mindlin-McNiven theory actually render less accurate results for the slender rod case $a/L = 1/20$ compared to the $a/L = 1/4$ case. This is the situation for the normal stress σ_{rr} along the central line $r = 0$ for the first mode, where certain terms do not properly cancel each other out using the Mindlin-McNiven theory. Hence, the stress magnitudes due to Mindlin-McNiven are on the same

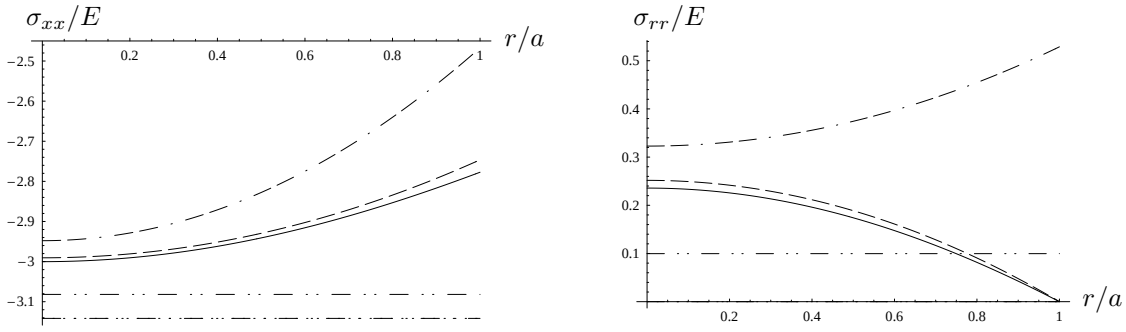

(a) σ_{xx} at $x = L$.

(b) σ_{rr} at $x = L$.

Fig. 2 Mixed boundary conditions: —— Exact, $---$ a^2, $-\,-\,\cdot\,-\,-$ M-McN, $-\,\cdot\,\cdot\,-$ M-H, $-\,\cdot\,-$ Love, $\cdots$ a^0.

level for both $a/L = 1/20$ and $a/L = 1/4$, see Fig.1(a), while the stress magnitudes for the other theories (including the exact) for the slender rod have decreased by more than a factor of ten. By choosing the correction coefficients κ_i differently (e.g. to unity) the result can be improved. This shows that the choice of the κ_i:s that render accurate dispersion curves in the low frequency regions does not necessarily result in the optimal stress distribution for this lowest eigenfrequency.

6.2 *Clamped boundary conditions*

Consider next the case when the rod is clamped in both axial and radial directions at both ends: $u_x = 0$ and $u_r = 0$ at $x = 0, L$. Of course, for a series expansion theory a^{2m} this means at both ends $u_k = 0$ for $k = 0, \cdots, 2m$ according to Section 4. As in the mixed boundary case, the three lowest eigenfrequencies are studied for $a/L = 1/20$ and $a/L = 1/4$, respectively. Since the exact solution can not be solved analytically, the eigenfrequencies using three dimensional theory may be approximated by the methods adopted in (**7**, **9**, **13**) as well as a higher order series expansion theory. In the latter case expansion of order a^{14} is used. For $a/L = 1/4$ the two lowest eigenfrequencies are given in (**7**, **9**, **13**) which is in accordance to the a^{14} results. The third eigenfrequency is also given by Buchanan (**13**), but here the third decimal actually differs from our results. The rate of convergence using the series expansion approach is rather slow in this case. However, as the final presented eigenfrequency is obtained for both the a^{12} and a^{14} theories, these results are assumed to have converged. A similar situation occurs for $a/L = 1/20$, where Liew and Hung (**9**) presents eigenfrequencies that also differ in the third decimal when compared to the

a^{14} results. Here the series expansion method converges already using the a^4 theory, and these results are thus believed to be correct.

The series expansion theories of different order are compared in Table 3. These results are quite similar to the mixed boundary case, see Table 1. The approximate theories are compared in Table 4. As in the previous case, these results show that the a^2 series expansion theory is generally superior to the traditional theories. Here the accuracies for these latter theories are inferior to the mixed boundary case. Moreover, both the Mindlin-Hermann and the Mindlin-McNiven theories are more accurate than Love's theory as expected. However, it is surprising that the simple classical a^0-theory renders results on the same accuracy level as the other more refined traditional theories.

a/L	Ω	a^{14}	a^0	a^2	a^4	a^6
$1/20$	Ω_1	0.3156	-4.4×10^{-3}	-3×10^{-4}	$*$	$*$
	Ω_2	0.6302	-3.0×10^{-3}	-5×10^{-4}	$*$	$*$
	Ω_3	0.9427	-2×10^{-4}	-5×10^{-4}	$*$	$*$
$1/4$	Ω_1	1.5942	-1.47×10^{-2}	-1.1×10^{-3}	$*$	2×10^{-4}
	Ω_2	3.0261	3.82×10^{-2}	-1.20×10^{-2}	2.7×10^{-3}	8×10^{-4}
	Ω_3	3.9300	1.991×10^{-1}	-1.04×10^{-2}	2.42×10^{-2}	-1.9×10^{-3}

Table 3 Clamped boundary conditions: The eigenfrequencies for the a^{14}-theory and the relative error for series expansion theories of order a^0, a^2, a^4 and a^6.

When presenting the distribution of stresses and displacements using the a^2 and classical theories for the lowest mode when $a/L = 1/4$, these results are to be compared to the series expansion theory of a high order. By inspection, the a^8 plots are indistinguishable from the a^{14} in the presumably worst case displayed, and thus the lower order is used for a comparison to simplify the numerics. Just as in the classic Filon's problem in statics, there are known to be stress singularities in the corners. Of course, none of the present rather low order theories are well suited for analyzing these effects. Hence, no plots are presented for the fields in these regions. Such end effects may be studied more in detail using various asymptotic boundary expansion methods, see further (**47**, **48**, **49**).

The plots are generally more dramatic in this boundary case than the previous mixed case. Figure

a/L	Ω	a^{14}	Love	M-H	M-McN	a^2
$1/20$	Ω_1	0.3156	-5.1×10^{-3}	3.8×10^{-3}	2.5×10^{-3}	-3×10^{-4}
	Ω_2	0.6302	-5.2×10^{-3}	3.0×10^{-3}	1.9×10^{-3}	-5×10^{-4}
	Ω_3	0.9427	-5.2×10^{-3}	2.0×10^{-3}	1.2×10^{-3}	-5×10^{-4}
$1/4$	Ω_1	1.5942	-2.81×10^{-2}	1.64×10^{-2}	1.03×10^{-2}	-1.1×10^{-3}
	Ω_2	3.0261	-1.51×10^{-2}	3.3×10^{-3}	-2.2×10^{-3}	-1.20×10^{-2}
	Ω_3	3.9300	7.26×10^{-2}	-2.4×10^{-3}	-1.60×10^{-2}	-1.04×10^{-2}

Table 4 Clamped boundary conditions: The eigenfrequencies for the a^{14}-theory and the relative error for approximate theories: Love, Mindlin-Hermann (M-H), Mindlin-McNiven (M-McN) and a^2-theory.

3(a) displays the variation of σ_{rr} at the central line $r = 0$ along the rod for different theories. In order to visualize the accuracies for these theories, the higher stresses at the ends are not included for scaling reasons. Instead such end effects are given in Figure 3(b). Both the Mindlin-McNiven and the a^2 theories are more or less equally correct in the interior Fig. 3(a), while more pronounced discrepancies close to the ends are illustrated in Fig. 3(b). Just as for the mixed boundary case, the stress σ_{xx} shows less pronounced variations between all the theories and is thus not displayed.

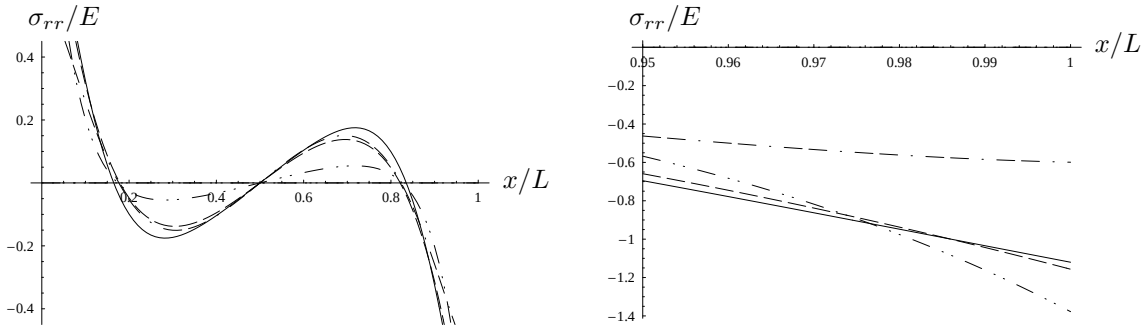

(a) σ_{rr} at $r = 0$.

(b) σ_{xr} at $r = 0$.

Fig. 3 Clamped boundary conditions: —— a^8, $---$ a^2, $--\cdot--$ M-McN, $-\cdots-$ M-H.

Figure 4 presents σ_{xx} and σ_{rr} at $x = 3L/4$, respectively. These results behave like in the mixed boundary case, albeit the a^2 theory is less accurate here. Note that the top horizontal line in Fig. 4(a) involves both the a^0 and the Love curves. As the rate of convergence is slower here than in the mixed boundary case, it is instructive to study the results from series expansion theories of different order. This

is illustrated for σ_{rr} at $x = 3L/4$ in Fig. 5(a). No plots are presented for σ_{xr} and σ_{rr} at $r = a$, since the different theories generally behave in a similar fashion as in the mixed case.

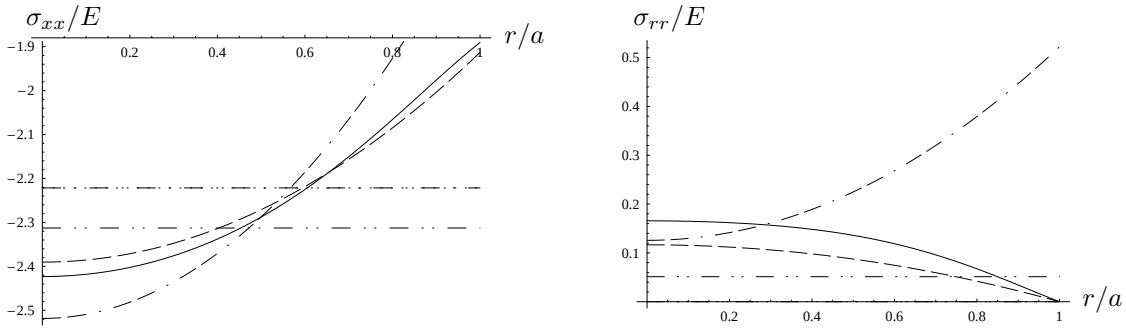

(a) σ_{xx} at $x = 3L/4$. (b) σ_{rr} at $x = 3L/4$.

Fig. 4 Clamped boundary conditions: —— a^8, $---$ a^2, $--\cdot--$ M-McN, $-\cdot\cdot\cdot-$ M-H, $-\cdot-$ Love, $\cdots$ a^0.

The clamped boundary case exhibits more variations in the displacements between the theories than the mixed boundary case, albeit these are still generally quite small. Figure 5(b) shows the behavior of u_x at $x = 3L/4$. Note that the a^0-curve is obtained by including the u_2-term in accordance with the discussion in Section 4. Hence, it is different to the constant u_0-value obtained for classical wave equation adopting the standard procedure. In the latter case the curve would clearly be on top the Love curve.

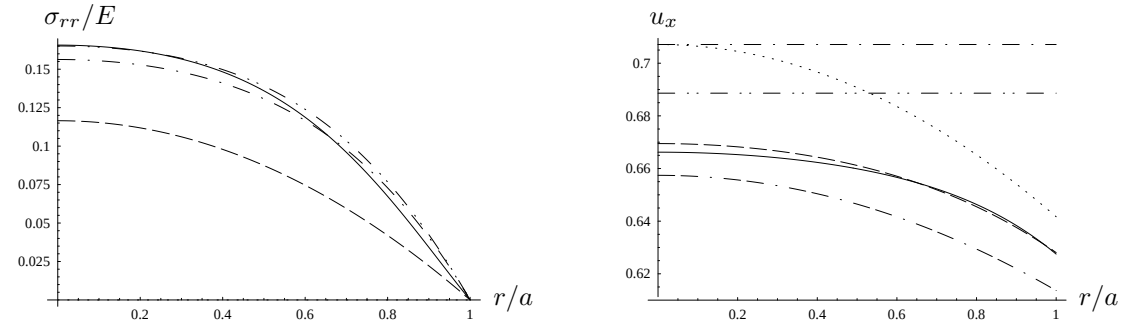

(a) —— a^8, $---$ a^2, $-\cdot-$ a^4, $-\cdot\cdot\cdot-$ a^6. (b) —— a^8, $---$ a^2, $--\cdot--$ M-McN, $-\cdot\cdot\cdot-$ M-H, $-\cdot-$ Love, $\cdots$ a^0.

Fig. 5 Clamped boundary conditions: σ_{rr} and u_x at $x = 3L/4$.

6.3 *Simple rod structures*

In this section two sets of boundary/coupling conditions are investigated explicitly: lateral boundary conditions varying along a homogeneous rod, and connected rods with varying radii. In both cases mixed end boundary conditions (guided ends) are assumed in order to accurately verify the results in the limit of a simple rod.

For the first case, consider an example where the rod is divided into a laterally free and a laterally clamped half. Hence, adopt equations (20) and (22) on $L_x = L_r = (0, L/2)$ with $\tilde{t}_x = \tilde{t}_r = 0$, as well as equations (21) and (23) on $L_x^* = L_r^* = (L/2, L)$ with $\tilde{u}_x = \tilde{u}_r = 0$. The $4m+2$ coupling conditions follow from Section 4.1 as termwise continuity conditions. When calculating the eigenfrequencies, these are converging at a slower rate than the standard cases presented in Sections 6.1–6.2. This expected behavior is readily seen in Table 5 which presents the lowest eigenfrequency when $a/L = 1/4$ for series expansion theories of the lowest orders. The results show that the eigenfrequency is higher than in the laterally free case as expected, see Table 1.

a/L	Ω	$m=0$	$m=1$	$m=2$	$m=3$
$1/4$	Ω_1	2.2284	2.4007	2.4400	2.4588

Table 5 The eigenfrequencies for series expansion theories of different order for laterally free/clamped boundary conditions with guided ends.

The displacement and stress distributions become more complicating than for the laterally free rod. For all the series expansion theories the lateral boundary conditions are exactly fulfilled along the rod, just as in the previous cases. However, there will also be a stress singularity at $x = L/2$ due to the abrupt transition from a free to a clamped boundary. As before, such features are not captured by the low order theories displayed here, even though pronounced stress levels are readily seen in the vicinity to this point. In conformity with the discussions on coupling conditions in Section 4.1, there will generally be discrepancies in the corresponding displacement and stress fields for the two halves at $x = L/2$, except for

σ_{xx}. Naturally, such discontinuities are zero when $r = 0$ (except for $m = 0$) and increase with the radius. Still these differences are quite small away from the singularity point $r = a$.

Figure 6(a) presents the variation of σ_{rr} along the rod when $r = 0$ for different series expansion theories. Clearly, the stress distribution is more complex than for the laterally free case Fig. 1(a). Concerning the lowest order equations $m = 0$, there is a jump discontinuity at $x = L/2$ as σ_{rr} is not modeled for a free lateral surface. Moreover, it could be noted that the laterally clamped rod equation in this simplest case is actually a one-dimensional Klein-Gordon equation.

Next, consider the case when two laterally free rods with identical material parameters are merged together at $x = L/2$: radius $a/2$ for $x < L/2$ and radius a for $x > L/2$. Using the $4m + 2$ coupling conditions presented in Section 4.1, the lowest eigenfrequency when $a/L = 1/4$ is given in Table 6 for series expansion theories of different orders. These seem to converge quicker than in the previous case.

a/L	Ω	$m = 0$	$m = 1$	$m = 2$	$m = 3$
$1/4$	Ω_1	1.5708	1.5491	1.5503	1.5506

Table 6 The eigenfrequencies for series expansion theories of different order for two radii with guided ends.

The displacement and stress distributions resemble in many cases the situation for a single laterally free rod, albeit being more complicating. Naturally, the lateral boundary conditions are exactly fulfilled for all the series expansion theories. Moreover, there will be a stress singularity at $x = L/2$ for $r = a/2$ due to the abrupt radius transition. Considering the normal stress σ_{xx} over $x = L/2$, this stress is not continuous as in the previous cases due to the generalized force continuity requirement. For higher order theories these discrepancies are gradually becoming smaller, albeit at a slow rate. Consequently, there are visible tendencies that both σ_{xx} and σ_{xr} are gradually approaching an ultimate stress-free condition for $r > a/2$ at $x = L/2$. Figure 6(b) presents the variation of σ_{rr} along the rod when $r = 0$ for different series expansion theories, and thus resembles Fig. 1(a). Note that there are small jump discontinuities for all orders at $x = L/2$. The normalization used in Fig. 6 is such that the longitudinal displacement u_x at

$r = 0$ is equal to unity at $x = L/2$. This is thus not its maximum value in either case, as that is slightly larger and occurs for x-values less than $L/2$.

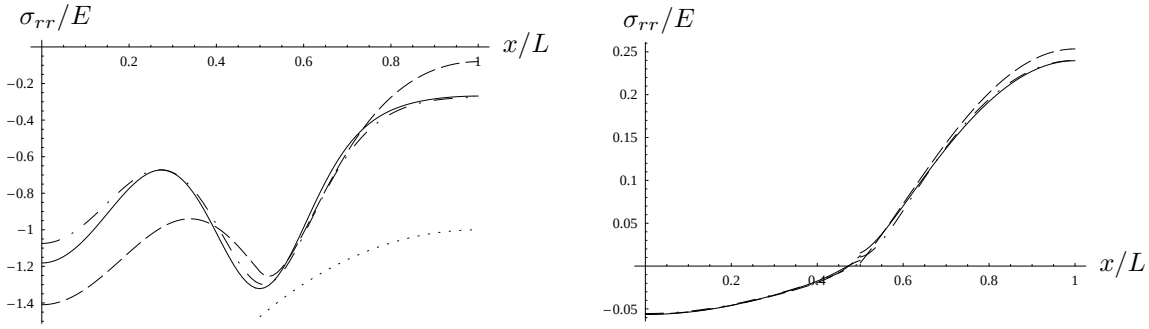

(a) Laterally free/clamped rod.

(b) Two rods with different radii.

Fig. 6 σ_{rr} at $r = 0$ with mixed end boundary conditions for $a/L = 1/4$. —— a^6, $\cdots$ a^0, $---$ a^2, $-\cdot-$ a^4.

As a final remark on how to deal with various sort of end/couple conditions, we have also studied an example of a laterally free homogeneous rod with guided ends at the inner radius $r < a/2$ and free ends at the outer radius $r > a/2$. Using notations according to (11)–(12), this is to say $R_{\{0,L\}r} = [0, a]$ with $\tilde{t}_r = 0$, and $R_{\{0,L\}x} = [0, a/2)$ with $\tilde{u}_x = 0$, as well as $R^*_{\{0,L\}x} = (a/2, a]$ where $\tilde{t}_x = 0$. However, this case resulted in severe difficulties on several levels. One question concerned how to mutually divide the $m + 1$ normal end boundary conditions between u_x and σ_{xx} on each end. Different combinations were tried up to order a^{10}, but all these resulted in numerical problems when identifying the lowest mode and its eigenfrequency. Moreover, the fulfilment of the prescribed end conditions were not adequately fulfilled simultaneously on both $R_{\{0,L\}x}$ and $R^*_{\{0,L\}x}$. This problem was investigated in some detail adopting various alternative approaches, without resulting in reliable results. Probably a much higher expansion order is needed to deal with such an involved end boundary condition. One alternative approach is here to separate the structure into one rod surrounded by a hollow cylinder, where the latter is modeled by the higher order series expansion equations described in (**35**).

7. Conclusions

This work presents the rod equation and corresponding boundary conditions to arbitrary order according to the power series expansion theory proposed by Boström. The method used is a generalized Hamilton's

principle resulting in variationally consistent equations that seem to be asymptotically correct. The equations are compared analytically to different traditional theories, and numerical results are presented for different rod structures. All theories are fairly adequate for calculating the eigenfrequencies, but the distribution of stresses varies considerably between theories.

Naturally the present approach for deriving both the differential equation and the corresponding boundary conditions can be applied to other structures. Based on the experiences from the present work, these results could thus be generalized systematically to other existing series expansions theories where the equations of motion and the recursion relations are known but not the end boundary conditions, e.g. for plates (**33**), shells (**35**), anisotropic rods (**36**, **37**), porous layers (**40**), and piezoelectric layers (**38**, **39**) . One application of such theories for structural elements is to implement them in finite element codes. These refined theories yield more accurate results than simpler traditional equations and at the same time the number of elements in a finite element code can be heavily reduced compared to using three-dimensional elements.

Acknowledgement

The authors wish to thank Anders Boström for important suggestions and interesting discussions during the preparation of the work. The constructive comments from the anonymous referees are also much appreciated.

References

1. K.F. Graff. *Wave Motion in Elastic Solids*. Clarendon Press, Oxford, 1975.

2. J.R. Hutchinson. Axisymmetric vibrations of a solid elastic cylinder encased in a rigid container. *J. Acoust. Soc. Am.*, 42:398–402, 1967.

3. J.R. Hutchinson. Axisymmetric vibrations of a free finite-length rod. *J. Acoust. Soc. Am.*, 51:233–240, 1972.

4. V.T. Grinchenko and V.V. Meleshko. Axisymmetric vibration of an elastic cylinder of finite length. *Sov. Phys. Acoust.*, 24:488–491, 1978.

5. J.R. Hutchinson. Vibrations of solid cylinders. *J. Appl. Mech.*, 47:901–907, 1980.

6. C. Fiedler and W. Wenzel. Analytical approximate 3D solution for the longitudinally vibrating cylinder. *Arch. Appl. Mech.*, 66:447–459, 1996.

7. L. Kari. Axially symmetric modes in finite cylinders – the wave guide solution. *Wave Motion*, 37:191–206, 2003.

8. P.R. Heyliger. Axisymmetric free vibrations of finite anisotropic cylinders. *J. Sound Vib.*, 148:507–520, 1991.

9. K.M. Liew and K.C. Hung. Three-dimensional vibratory characteristics of solid cylinders and some remarks on simplified beam theories. *Int. J. Solids Struct.*, 32:3499–3513, 1995.

10. A.W. Leissa and J. So. Comparisons of vibration frequencies for rods and beams from one-dimensional and three-dimensional analyses. *J. Acoust. Soc. Am.*, 98:2122–2135, 1995.

11. A.W. Leissa and J. So. Accurate vibration frequencies of circular cylinders from three-dimensional analysis. *J. Acoust. Soc. Am.*, 98:2136–2141, 1995.

12. G.M.L. Gladwell and U.C. Tahbildar. Finite element analysis of the axisymmetric vibrations of cylinders. *J. Sound Vib.*, 22:143–157, 1972.

13. G.R. Buchanan. Frequencies and mode shapes for finite length cylinders. *J. Sound Vib.*, 246:927–941, 2001.

14. A.E.H. Love. *A Treatise on the Mathematical Theory of Elasticity*. Cambridge University Press, London, 1927.

15. R.D. Mindlin and G. Hermann. A one-dimensional theory of compressional waves in an elastic rod. *Proc. 1st U.S. Natn. Congr. Appl. Mech.*, pages 187–191, 1950.

16. R.D. Mindlin and H.D. McNiven. Axially symmetric waves in elastic rods. *J. Appl. Mech.*, 27:145–151, 1960.

17. E. Volterra and E. C. Zachmanogiou. *Dynamics of Vibrations*. Charles E. Merrill Books, Ohio, 1965.

18. J.B. Haddow, R.J. Tait, and T.B. Moodie. A theory for high-frequency longitudinal waves in bars. *Q. Jl. Mech. appl. Math.*, 37:143–160, 1984.

19. S.P. Anderson. Higher-order rod approximations for the propagation of longitudinal stress waves in elastic bars. *J. Sound Vib.*, 290:290–308, 2006.

20. M. Krawczuk, J. Grabowska, and M. Palacz. Longitudinal wave propagation. Part I – Comparison of rod theories. *J. Sound Vib.*, 295:461–478, 2006.

21. J.D. Achenbach and S.J. Fang. Asymptotic analysis of the modes of wave propagation in a solid cylinder. *J. Acoust. Soc. Am.*, 47:1282–1289, 1970.

22. A. Boström. On wave equations for elastic rods. *Z. Angew. Math. Mech.*, 80:245–251, 2000.

23. R.D. Mindlin. High frequency vibrations of crystal plates. *Q. Appl. Math.*, 19:51–61, 1961.

24. M.A. Medick. One-dimensional theories of wave propagation and vibrations in elastic bars of rectangular cross section. *J. Appl. Mech.*, 33:489–495, 1966.

25. M.W. Johnson and O.E. Widera. An asymptotic dynamic theory for cylindrical shells. *Stud. appl. Math.*, 48:205–226, 1969.

26. K. Hirano and K. Hirashima. Formulation and accuracy of the circular cylindrical shell theory due to higher order approximation. *JSME Int. J., Series I*, 32:337–340, 1989.

27. H. Matsunaga. The application of a two-dimensional higher-order theory for the analysis of a thick elastic plate. *Comp. Str.*, 45(4):633–648, 1992.

28. J.G. McDaniel and J.H. Ginsberg. Thickness expansions for higher-order effects in vibrating cylindrical shells. *J. Appl. Mech.*, 60:463–469, 1993.

29. K.P. Soldatos. Generalization of variationally consistent plate theories on the basis of a vectorial formulation. *J. Sound Vib.*, 183:819–839, 1995.

30. I.T. Selezov. Hyperbolic models of wave propagation in rods, plates, and shells. *Izv. RAN. Mekhanika Tverdogo Tela*, 29:64–77, 1994.

31. N.A. Losin. Asymptotics of flexural waves in isotropic elastic plates. *J. Appl. Mech.*, 64:336–342, 1997.

32. F.I. Niordson. An asymptotic theory for circular cylindrical shells. *Int. J. Solids Struct.*, 37:1817–1839, 2000.

33. A. Boström, G. Johansson, and P. Olsson. On the rational derivation of a hierarchy of dynamic equations for a homogeneous, isotropic, elastic plate. *Int. J. Solids Struct.*, 38:2487–2501, 2001.

34. M. Johansson, P.D. Folkow, A.M. Hägglund, and P. Olsson. Approximate boundary conditions for a

fluid-loaded elastic plate. *J. Acoust. Soc. Am.*, 118:3436–3446, 2005.

35. A.M. Hägglund and P.D. Folkow. Dynamic cylindrical shell equations by power series expansions. *Int. J. Solids Struct.*, 45:4509–4522, 2008.

36. P.A. Martin. Waves in wood: axisymmetric waves in slender solids of revolution. *Wave Motion*, 40:387–398, 2004.

37. P.A. Martin. On flexural waves in cylindrically anisotropic elastic rods. *Int. J. Solids Struct.*, 42:2161–2179, 2005.

38. G. Johansson and A.J. Niklasson. Approximate dynamic boundary conditions for a thin piezoelectric layer. *Int. J. Solids Struct.*, 40:3477–3492, 2003.

39. K. Mauritsson, A. Boström, and P.D. Folkow. Modelling of thin piezoelectric layers on plates. *Wave Motion*, 45:616–628, 2008.

40. P.D. Folkow and M. Johansson. Dynamic equations for fluid-loaded porous plates using approximate boundary conditions. *J. Acoust. Soc. Am.*, 125:2954–2966, 2009.

41. K. Washizu. *Variational methods in elasticity and plasticity*. Pergamon Press, 1982.

42. R.B. Hetnarski and J. Ignaczak. *Mathematical theory of elasticity*. Taylor & Francis, 2004.

43. A.C. Eringen and E.S. Şuhubi. *Elastodynamics Vol. II, Linear theory*. Academic Press, 1975.

44. Y.Y. Yu. *Vibrations of Elastic Plates: Linear and nonlinear dynamical modeling of sandwiches, laminated composites, and piezoelectric layers*. Springer-Verlag, New York, 1996.

45. J.D. Achenbach. *Wave Propagation in Elastic Solids*. North-Holland, Amsterdam, 1973.

46. N.A. Losin. On the equivalence of dispersion relations resulting from Rayleigh-Lamb frequency equation and the operator plate model. *J. Vibr. Acoust.*, 123:417–420, 2001.

47. J.P. Benthem and P. Minderhoud. The problem of the solid cylinder compressed between rough rigid stamps. *Int. J. Solids Struct.*, 8:1027–1042, 1972.

48. R.D. Gregory and F.Y.M. Wan. Correct asymptotic theories for the axisymmetric deformation of thin and moderately thick cylindrical shells. *Int. J. Solids Struct.*, 30:1957–1981, 1993.

49. J.D. Kaplunov, L.Y. Kossovich, and E.V. Nolde. *Dynamics of thin walled elastic bodies*. Academic Press, 1998.